CHAPTER 5

Luminescence and Photovoltaic Effects in Polymer-Based Nanocomposites

L. Bakueva, S. Musikhin, E. H. Sargent
Department of Electrical and Computer Engineering, University of Toronto, Toronto M5S 3G4, Canada

H. E. Ruda, A. Shik
Energenius Centre for Advanced Nanotechnology, University of Toronto, Toronto M5S 3E4, Canada

CONTENTS

1. Introduction 182
2. Technological Aspects 182
   2.1. Nanocrystals and Core–Shell Structures 182
   2.2. Polymer–Nanocrystal Composites 184
   2.3. Device Structures 184
3. Energy Band Diagram 185
4. Photoelectric Properties of Conducting Polymers 186
5. Experimental Investigations of Polymer–Nanocrystal Composites 190
   5.1. Nonequilibrium Carriers in Nanocomposites 190
   5.2. Photoconductivity 192
   5.3. Photo- and Electroluminescence 196
6. Theory of Polymer–Nanocrystal Light Emitters 201
   6.1. Potential Profile and Carrier Capture for a Single Nanocrystal 202
   6.2. General Expressions 202
   6.3. Current–Voltage Characteristic 203
   6.4. Quantum Yield of Nanocrystal Luminescence 204
7. Theory of Photoelectric Phenomena in Type-II Composites 205
   7.1. Band Diagram Under Illumination 206
   7.2. Recombination Rate 207
8. Other Device Applications 208
   8.1. Gas Sensors 208
   8.2. Nanoscale Circuits 209
9. Conclusion 209
   Appendix: Conjugated Polymers Most Often Used in Nanocomposites 210
   References 213

ISBN: 1-58883-029-2 / $35.00
Copyright © 2003 by American Scientific Publishers
All rights of reproduction in any form reserved.

Handbook of Organic–Inorganic Hybrid Materials and Nanocomposites
Volume 2: Nanocomposites
Edited by H. S. Nalwa

1. INTRODUCTION

Conducting polymers as materials for light-emitting and photovoltaic devices have been the subject of considerable interest over the last decade (see, e.g., [1, 2]). Because of their light weight and excellent mechanical properties, they are ideal candidates for applications which require portability. The ease of processability and flexibility in the thin film form of polymers (e.g., spin-on or ink-jet printed deposition [3]) contrasts with the stringent requirements of vacuum epitaxial growth of monocrystalline semiconductor structures. Flexible substrates lend themselves to innovative designs for end products and processing based on continuous coating of large-area surfaces. This physical flexibility is matched by functional versatility: a wide variety of compounds can be fashioned using synthetic methods, with energy gap and ionization potential being tuned by chemical modification of polymer chains.

A new degree of freedom has been introduced to the realm of conducting polymers: the incorporation of an inorganic component in order to form composite structures. The influence of inclusions is at least twofold:

- Inclusions create areas with high intensity of generation and recombination of nonequilibrium carriers. In photoelectric devices, this may result in a considerable increase in the quantum yield and the additional possibility of tuning spectral characteristics.
- Inclusions modify characteristics of the surrounding polymer, influencing the optical, photoelectric, and transport properties of the composite.

In this chapter we review experimental reports in this actively developing area, give a theoretical description of observed phenomena, and discuss possibilities of further optimization of light-emitting and photovoltaic devices based on the conducting polymer/inorganic nanocrystal composites.

This choice of materials leaves outside the scope of our consideration a great number of interesting works on optical properties of composites using ordinary, nonconducting polymers (such as PMMA and many others). We also will not consider polymers with ionic conductivity (see, e.g., [4, 5]) where the physics of charge transfer differs essentially from the objects of our primary interest.

2. TECHNOLOGICAL ASPECTS

In this section we briefly discuss the fabrication of organic–inorganic nanocomposites. We will not consider here the chemical aspects of synthesizing conducting polymers used as the matrix material. A list of the most popular conducting polymers used for nanocomposites is given at the end of the chapter. The description of corresponding chemical processes, different for different polymers, can be found elsewhere. A great number of conducting polymers are now commercially available and can be directly used for fabrication and investigation of polymer-based composites. For this reason we discuss below only problems related to nanocrystal fabrication and their embedding into the polymer matrix.

2.1. Nanocrystals and Core–Shell Structures

There exist a number of different methods of nanocrystal fabrication briefly mentioned, for example, in [5]. We restrict our attention to those from which nanocrystals are obtained in a form suitable for subsequent incorporation into polymer films, for instance, in some organic solutions. This narrows the choice of technological possibilities chiefly to a variety of techniques based on organometallic and polymer chemistry [5, 6]. We consider the main principles of nanocrystal fabrication using as an example II–VI semiconductor compounds (CdSe, CdS, ZnSe, etc.)—the most popular materials used for this purposes. These may be fabricated via chemical reaction in solution between metal alkyls containing group II metals (dimethylcadmium, diethylzinc, etc.) and organophosphine chalcogenides or bistrimethylsilylchalcogenides supplying the group VI elements.

To grow monodisperse nanocrystals of a given size, it is necessary to control the process of nucleation and subsequent growth of nanocrystals. Many works in this direction are based on the old classical work of La Mer and Dinegar [7] who showed that the production of monodisperse nanocrystals requires a temporally discrete nucleation event followed by slower controlled growth around the existing nuclei. Rapid addition of reagents to the reaction vessel raises the precursor concentration above the nucleation threshold. A short nucleation burst partially relieves the supersaturation. As long as the consumption of feedstock by the growing colloidal nanocrystals is not exceeded by the rate of precursor addition, no new nuclei form. Since the rate of growth for all of the nanocrystals is similar, the initial size distribution is largely determined by the time over which nuclei are formed and begin to grow. If the percentage of growth during the nucleation period is small compared with subsequent growth, the nanocrystals can become more uniform over time. This phenomenon has been referred to as focusing of the size distribution and is due to the strong size dependence of the crystal surface energy influencing the kinetics of crystal growth [8]. Direct observations confirmed more than twofold (from 20% to 7.7%) narrowing of the size distribution due to the "focusing" phenomenon in CdSe nanocrystal growth [9].

Focusing of the size distribution occurs when the nanocrystals present in solution are slightly larger than the equilibrium critical size. Under these conditions, the smaller nanocrystals grow faster than the larger ones. When the concentration of material in solution is depleted due to growth, the critical size becomes larger, and the distribution broadens because some smaller

nanocrystals are shrinking and eventually disappear while larger ones are still growing. This is known as Ostwald ripening [10], or defocusing.

Nanocrystal growth can be operated by two methods: (i) fast injection of the metal-organic precursors and (ii) using different kinds of coordinating solvents. A rapid precursor injection in a hot (~150–350 °C) solution triggers the supersaturation and subsequent nucleation and gives rise to a homogeneous nucleation, which, followed by a slow growth and annealing, results in a uniform surface derivatization. The role of coordinating solvents consists in terminating the particle surface with organic ligands. This treatment on the one hand modifies and stabilizes the nanocrystal surface, increases their solubility, and prevents agglomeration among particles and, on the other hand, controls the density of surface states and decreases surface recombination. The solvents usually used are mixtures of long-chain alkylphosphines, alkylphosphine oxides, alkylamines, etc. [10, 11].

When the stabilizing molecules are attached to the nanocrystal surface as a monolayer through covalent or ionic bonds, they are referred to as capping groups [12]. The above-mentioned stability with respect to aggregation occurs only if the capping groups provide a repulsive force strong enough to counteract the internanocrystal van der Waals attraction. If the capping groups are well bound to the surface of nanocrystals, the resulting powders are stable in a variety of organic solvents, which is important for their storage and further use for fabrication of polymer–nanocrystal composites.

The methods of ultimate control of the nanocrystal size can be divided into two main categories (see [13]): one in which the size is controlled by the relative concentration of the capping material [14] and the second method in which the ultimate cluster size is dictated by the size of a reverse micelle inside which the particle is grown [15] (see Fig. 1).

These methods were successfully applied for growing of nanocrystals CdS [6, 13, 16, 17], CdSe [16, 18–23], CdTe [17, 24], ZnSe [23], $Cd_{1-x}Zn_xS$ [17], $Cd_{1-x}Mn_xS$ [17], and $Cd_{1-x}Mn_xSe$ [25] followed by fabrication of nanocomposites using different kinds of conducting polymers. By changing the growth conditions, the authors managed to vary the mean nanocrystal size from approximately 10 to 100 Å and beyond. Direct measurements by transmission electron microscopy, atomic force microscopy, and small-angle X-ray scattering confirmed that in many cases almost monodisperse size distribution (down to<5% standard deviation [26]) could be achieved (Fig. 2). This key result is independently confirmed by measurements of luminescent spectra described in Section 5.

In addition to II–VI compounds, the methods described were used for fabrication of nanocrystals and nanocomposites from some other semiconductors. Synthesis of InP and InAs has been achieved by rapidly mixing and heating group III and V precursors in boiling coordinating solvents [27–29]. Nanocrystals $Al_xGa_{1-x}N$ [30], GaSb [31], Ge [32], Si [33], PbS [34], and Ag_2S [17] in organic solvents have also been fabricated. Some of them used different technological approaches more adequate for a particular semiconductor. For instance, Si nanocrystals [33] were developed by means of a high-temperature gas-phase synthesis using disilane pyrolysis. In this procedure, nucleation, growth, annealing, and surface derivatization take place in the aerosol state at approximately 1000 °C, which is favorable to producing the most thermodynamically stable isomer. For production of GaSb nanocrystals [33] the process is based on the chemical reaction between $GaCl_3$ and $Sb(SiMe_3)_3$ in different solvents.

So far we have described the growth of semiconductor nanocrystals for semiconductor–polymer composites. However, a series of interesting phenomena with possible device applications is observed in dielectric–polymer composites as well (see Section 5 below). Thus it is worth briefly mentioning also the case of dielectric nanocrystals.

Usually the size and quality requirements for dielectric nanocrystals are less rigid. In semiconducting nanocrystals, which are intended to play the role of potential wells for electrons and holes (see Section 3), the size should be small and carrier mobility high enough to provide effective quantization of the electron and hole energy spectra [5]. For many applications, particularly for light-emitting devices, additional requirement of a small size

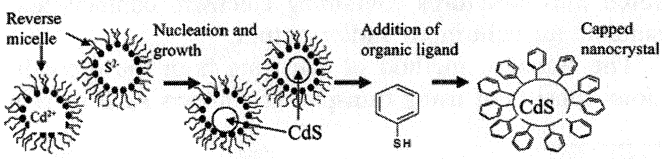

Figure 1. Synthesis of CdS nanocrystals. Reprinted with permission from [13], J. G. Winiarz et al., *Chem. Phys.*, 245, 417 (1999). © 1999, Elsevier Science.

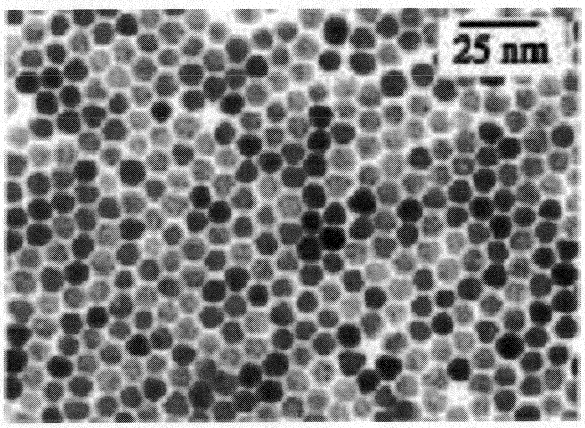

Figure 2. High resolution TEM-image of 8.5 nm diameter CdSe nanocrystals. Reprinted with permission from [9], X. Peng et al., *J. Am. Chem. Soc.*, 120, 5343, (1998). © 1998, American Chemical Society.

dispersion exists to provide a narrow spectrum of emitted light. Dielectric inclusions instead typically play the role of potential bumps, repelling carriers. For this reason, dielectric nanocrystals for the polymer-based composites are often prepared by rather simple chemical reactions in solution [35–37] or even chosen from commercially available nanocrystals of different oxides [38–40].

Among dielectric inclusions, one material should be mentioned separately, namely, titanium oxide (TiO_2). This material plays an active and important role in photoelectric phenomena, considerably improving characteristics of the polymer-based solar elements, which will be discussed in Section 5. For this reason, technology of TiO_2 nanocrystals is the object of special concern described, for example, in [41–44].

Fabrication of nanocrystals with a given chemical composition and size distribution is not the only technological problem to be solved on the way to finding nanocomposites suitable for device applications. The next serious problem consists of reducing the powerful recombination effects at the nanocrystal surface.

There are two main methods of suppressing surface recombination, often used in tandem. One relates to surface passivation and has already been partially discussed. The most popular passivating agents widely used for II–VI nanocrystals are trioctylphosphine (TOP) and trioctylphosphine oxide (TOPO).

The other method consists of replacing chemically homogeneous (or homostructure) nanocrystals with core–shell structures. These are two-phase nanocrystals consisting of an internal core semiconductor with bandgap E_{g1} of radius several nanometers, covered by a layer of a larger bandgap ($E_{g2} > E_{g1}$) material. The thickness of this shell layer does not exceed several lattice constants (1–2 nm). Since the core material presents a potential well for carriers, the electron and hole wave functions are confined mostly inside the core material and their amplitude at the external surface of nanocrystals is rather small. This may reduce noticeably recombination at this surface as long as the core–shell interface for proper fabrication technology provides a nearly ideal heterojunction causing no additional undesirable recombination.

Growth of core–shell structures is based on the same standard procedure of pyrolysis of organometallic reagents used for fabricating chemically uniform nanocrystals as described above. After the core part is grown, a fresh solution of solvent and stabilizers is added. The solution is then heated while precursors for the shell are gradually added [6, 21]. The rate of new precursor addition should not exceed the rate of deposition on the seed in order not to grow separate crystals of the shell phase. The second growth stage is usually performed at lower temperature to avoid growth of the core material.

The most popular core–shell nanocrystals used in polymer-based composites consist of CdSe core ($E_{g1} =$ 1.7 eV [45]) and CdS shell ($E_{g2} = 2.5$ eV) [46, 47]. Core–shell structures CdSe/ZnS [11, 22, 48, 49], CdSe/ZnSe [50], CdS/ZnS [49], and InAs/ZnSe [51] have also been reported.[1] Recent work [51] reports core and shell materials of different semiconductor groups (II–VI and III–V) grown by a two-step pyrolysis of organometallic precursors thoroughly described in [54].

2.2. Polymer–Nanocrystal Composites

Uniform or core–shell nanocrystals are stored in solution with a proper stabilizer chemically compatible with the materials used in synthesis of the polymer matrix. The method of preparation of polymer-based composites depends on the structure of nanocomposites we want to obtain.

The most common approach consists in mixing the polymer and nanocrystal-containing solutions followed by spin coating on the substrates and, in some cases, also the final thermal annealing [16, 20, 22, 55–57]. This method results in a composite with nanocrystals randomly distributed over the whole matrix volume.

In some cases, especially for light-emitting structures, it is desirable to concentrate most nanocrystals in a thin layer compared with the total thickness of the polymer film (see Section 5.4). In this case polymer and nanocrystal solution are spin coated separately in two consequent operations [21, 58].

It is also possible to use more sophisticated methods of growing partially or completely ordered nanocomposite structures. For instance, in [59, 60] the layer-by-layer self-assembly method was described and applied to fabricate a composite with CdTe nanocrystals for electroluminescent devices. The driving force in the method is the electrostatic attraction between oppositely charged molecules, which, in turn, appear in the process of consecutive adsorption of polyanion and polycation monolayers. Some interesting aspects of a complete two- and three-dimensional self-organization of CdSe nanocrystals can also be found in [61].

2.3. Device Structures

Fabrication of separate films of polymer–nanocrystal composites described above is an essential but not ultimate goal in the direction of device realization. For most experimental measurements, as well as for light-emitting and photovoltaic devices, these films should be incorporated into structures containing electrical contacts and suitable for light input and/or output.

The standard method of satisfying both these conditions consists of using transparent contacts such as thin

[1] Nanostructures containing a wide-gap core with a narrow-gap shell can be also fabricated [52, 53]. These physically interesting "quantum shell" systems are, however, less promising for optoelectronic applications and will not be discussed here.

films of a mixed indium–tin oxide (ITO). This material widely used in optoelectronic devices possesses a high (up to 10^{21} cm^{-3}) concentration of free carriers and thus a low resistance and simultaneously is transparent in the spectral region 350–1100 nm [38–40]. Figure 3 shows the standard simple structure used for both physical investigations and fabrication of light-emitting devices. It consists of an optically transparent substrate such as glass or polymer film, if the device should be mechanically flexible, covered by a thin layer of ITO. By using technological methods described in the previous subsection this substrate is covered by the film of polymer–nanocrystal composite. The second contact is deposited on top of the composite layer. The upper electrode can be nontransparent and is usually a simple metallic layer.

If an external bias is applied to the structure, electrons injected from a cathode and holes injected from an anode are captured by nanocrystals and recombine there with the emission of light. The theory of this process considered in Section 6 predicts that for the quantum yield of electroluminescence to have a maximal value, the injection currents of electrons and holes should be equal. This creates serious restrictions for the choice of electrode materials. As will be shown in the next section, most conducting polymers are characterized by rather low values of the electron affinity χ^p and most metals, as well as ITO, can provide effective hole and weak electron injection into the polymer matrix. For this reason, ITO is used as an anode and the main problem consists of creating a cathode with a comparable effectiveness of electron injection. This restricts the choice of cathode material to metals with low work function W such as Li ($W = 2.38$ eV), Ca ($W = 2.8$ eV), Mg ($W = 3.64$ eV) and Al ($W = 4.25$ eV) [62]. Some of these low-work-function metals are unstable in the ambient atmosphere and are usually covered by a protecting layer of Al or Ag.

The effectiveness of electron injection can also be increased by creating an additional dielectric layer between the polymer and metal, thin enough not to block the current completely [63–65]. The most probable explanation for this phenomenon [66] is the fact that the voltage drop at this layer shifts the Fermi level in the metal relating to molecular orbitals in the polymer and decreases the barrier to electron injection.

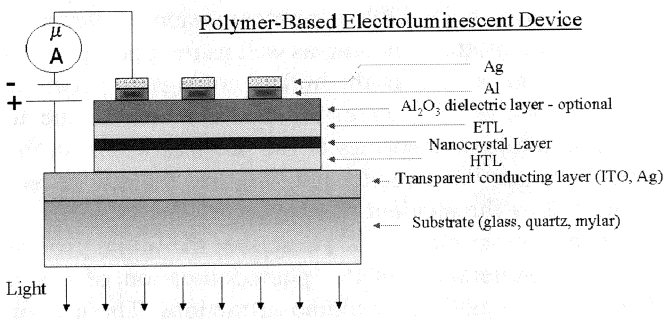

Figure 3. Schematic construction of a polymer-based light-emitting device. ETL—electron transport layer, HTL—hole transport layer.

3. ENERGY BAND DIAGRAM

Luminescence and photovoltaic phenomena in polymer–nanocrystal composites described in the present chapter are complicated processes. They rely on optical generation of nonequilibrium carriers (for photovoltaic phenomena or photoluminescence) or their injection from contacts (for electroluminescence), carrier transport though the polymer matrix, their capture to and emission from nanocrystals, and recombination inside nanocrystals as well as in the polymer matrix. The description of all these phenomena requires the knowledge of the electron and hole spectrum both in the matrix and in nanocrystals and their relative position at the polymer–nanocrystal interfaces.

The band diagrams of semiconductors and dielectrics are usually well known, not only in bulk materials but also with the account of possible size quantization in very small nanocrystals (see, e.g., [5]). For conducting polymers, it may suffice to know the positions of the highest occupied molecular orbital (HOMO) and the lowest unoccupied molecular orbital (LUMO) which play roles similar to the valence and conduction bands in a semiconductor [67]. This analogy between semiconductors and conducting polymers can be very fruitful for qualitative understanding of most observed phenomena but there exist two serious distinctions between these two types of materials. These play an essential role in our further interpretation of experimental results.

- The HOMO and LUMO energies contain an appreciable polarization component, which is determined by long-range Coulomb forces and can be modified in highly dispersed nanocomposites.
- Carrier mobilities in conducting polymers are many orders of magnitude lower than in semiconductors and usually differ drastically for electrons and holes.

Most electronic phenomena in composites depend to a great extent on the relative values and relative positions of the bandgap in a semiconductor (or dielectric) E_g^s and the HOMO–LUMO gap in a polymer E_g^p. The particular energy band diagram depends on the relationship between E_g^s and E_g^p as well as on the electron affinities of both materials χ^s and χ^p. Figure 4 shows all the qualitative band alignment possibilities. Available literature data give for most conducting polymers χ^p ranging from 2.3 to 2.6 eV [1]. This is less than the typical electron affinity for most semiconductors which are usually close to 4 eV [45] and for a number of dielectrics (e.g., TiO_2 with $\chi^s = 4.2$ eV [67]). For this reason, the band diagrams (c) and (f) are presumably not realized in polymer-based composites and will not be discussed below.

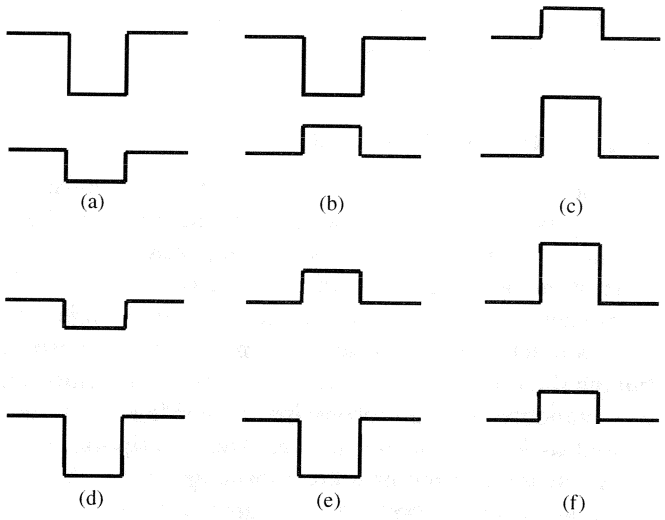

Figure 4. Different possible energy band diagrams of polymer–semiconductor (a,b,c) and polymer–dielectric (d,e,f) composites. (b) and (e) correspond to type-I and all others to type-II band diagrams.

The four remaining diagrams can be classified according to two characteristics. The first one is the ratio E_g^s/E_g^p. We will refer to the case of narrow-gap inclusions $E_g^s < E_g^p$ [(a) and (b)] as that of polymer–semiconductor composites and refer to the opposite situation $E_g^s > E_g^p$ [(d) and (f)] as the polymer–dielectric composites. The other characteristic is the relative position of gaps. One gap may lie completely inside the other [(b) and (e)] or form a staggered structure [(a) and (d)]. In the physics of semiconductor heterojunctions, the first situation is called type-I band alignment and the second situation type-II.

For the band diagram (b), semiconductor nanocrystals play the role of potential wells for both electrons and holes. This construction has definite advantages for light-emitting devices, such as LEDs and lasers. The concentration of nonequilibrium electrons and holes in the same confined regions results in increased efficiency and decreased threshold currents in these devices.

Another important class of devices—photovoltaic structures, including solar elements—benefits from different band alignment. These devices are based on spatial separation of photogenerated electrons and holes in an electric field, resulting in the flow of electric current in an external circuit. For this purpose the band diagram (b) is not optimal since both electron and holes concentrated in semiconductor inclusions require for their separation additional activation into the polymer matrix, which may suppress the effectiveness of photovoltaic devices. On the contrary, in the type-II band diagram [(a) or (d)] such barriers are absent, at least for one type of carrier, presenting an advantage in photovoltaic applications.

We discuss in detail the implications of band alignments in Sections 5 and 6 for type-I and in Sections 5 and 7 for type-II structures.

The band diagrams shown in Figure 4 correspond to an idealized picture. In real systems it may be considerably distorted by at least two important factors. One of them is the electrostatic band modulation when nonequilibrium carriers are partially separated by the potential relief and nanocrystals acquire some electric charge. This effect is important in type-II systems and will be considered in detail in Section 7.

The other difference from the idealization of Figure 4 comes from changes in polarization energy caused by nanocrystals. In conducting polymers, polaron effects play a very important role [67], shifting the energy levels and decreasing the effective HOMO–LUMO gap E_g^p. This polaron shift W is caused by interaction between an electron at the given atom with surrounding atoms including not only nearest neighbors but also atoms from higher coordination spheres. For polymer molecules in the closest vicinity of nanocrystals, some of these polarizing units are replaced by different molecules with different polarizability α. It will result in a local decrease of E_g^p for the case when α_I exceeds the polarizability of the polymer matrix and in an increase of E_g^p in the opposite case, accompanied by corresponding changes in the luminescence spectra [40].

4. PHOTOELECTRIC PROPERTIES OF CONDUCTING POLYMERS

Since the main applied prospects of conducting polymer–nanocrystal composites are related to optoelectronics and, particularly, to light-emitting and photovoltaic devices, we focus this chapter on experimental results of luminescent and photoelectric phenomena as well as key electrical, primarily current–voltage, characteristics. We begin by summarizing these phenomena in pure conducting polymers allowing us to reveal subsequently the impact of nanocrystals.

Photoconductivity phenomena in conjugated polymers are discussed in detail in [68, 69]. The nature and spectrum of light-induced electron excitation play a central role in these phenomena. The analysis of the photocurrent response of metal/polymer/metal structures has been established to be a powerful method for the investigation of injection of holes [70] or photoemission of electrons [71] over a Schottky junction, as well as the photogeneration of charge carriers in the bulk of conjugated polymers [72, 73]. In the latter case, the photocurrent is due to mobile photoexcited species of the polymer which, in the semiconductor band model [74, 75], are directly photogenerated by the incident photons.

The exciton model [76, 77] describes the initial process of carrier generation as the photogeneration of a singlet exciton bound by Coulomb attractions. The exciton must be broken to obtain free carriers that can migrate in an external applied electric field. Excitons can be either

intrachain singlet excitons localized within the same conjugation length (segment of polymer chain) or interchain excitons (bound polaron pairs) with electrons and holes localized at different chain segments or even at different chains, differing from singlet excitons by their binding energy. In interchain excitons, the wave functions of negative and positive polarons overlap weakly, so that the probability of radiative recombination is low and the main recombination channel is the nonradiative geminal recombination.

Picosecond photoinduced absorption studies [78, 79] show that electron excitations in conducting polymers are mostly polaron pairs and only about 10% of them are excitons. The decay of polaron pairs can be caused by jumping of one charge on the adjacent chain followed by formation of a polaron pair or of an exciton which subsequently decays; the positive and negative polarons move randomly on their own chains and separate thermally or in the presence of an electric field, yielding free polarons contributing to photocurrent. The polaron ($P^{\pm}$) pairs can also evolve to bipolarons ($BP^{\pm}$). The direct reaction $P^{\pm} + P^{\pm} = BP^{\pm}$ is hindered by a strong Coulomb repulsion, but the residual impurities and dopants can facilitate this process [80]. Once appearing, the bipolaron is a more stable formation than the polaron.

Formation of inter- and intrachain excitons is caused by the generation process itself. It occurs when the excess photon energy considerably exceeds the exciton binding energy, causing exciton heating, as well as to the mutual orientation of the photon polarization vector and the polymer chain segment. The intrinsic optical properties of polymers are found to be highly anisotropic [81] due to their quasi-one-dimensional nature. Photoexcitation with the parallel polarization creates predominantly intrachain electron–hole pairs, while the perpendicular polarization generates interchain pairs. In the last case, delocalized excited states (Wannier-like excitons) are formed [82], where the pair constituents are situated on different chains or on different conjugation lengths of the same chain. The absorption coefficients for parallel and perpendicular polarization of light relating to the direction of a chain segment differ noticeably, with much higher absorption for the parallel orientation [83, 84]. For this reason, the absorption coefficient in amorphous, nonoriented polymer films almost coincides with that for parallel polarization. At high photon energies, exceeding the bandgap 2.5–3 times, the absorption anisotropy drops.

The breaking of electron–hole pairs is assisted by extrinsic mechanisms such as a heterojunction between two polymers of different carrier mobility [85], or via chemical defects such as oxygen and carbonyl [79], or via applied and built-in electric field and temperature. The pair break in the electric field is often described by Onsager's theory of geminate pair dissociation [85]. A photon of sufficient energy is assumed to have generated a Coulombically bound electron and hole (geminate pair) which thermalize at a separation distance r_0. This initial separation distance increases with photon energy. Whether they dissociate into a pair of free carriers or recombine to form an exciton is determined by r_0 and by their subsequent diffusion in the electric field, which is a superposition of the Coulomb well due to their attraction, and the applied field. The theory predicts that electron–hole dissociation is an activated process, with the activation energy decreasing with increasing field. The field dependence predicted is steep over a wide range of fields [68]. This theory with subsequent modifications [86] describes pair breaking in molecular crystals but fails to describe the processes in polymers [87]. It fails in particular to explain the weak temperature dependence. The dissociation of optical excitations in conjugated polymers is described much better with the theory suggested in [88, 89]. The model of temperature-independent photogeneration of charge carriers in conjugated polymers is based on the concept of the on-chain dissociation of unrelaxed higher optical excitations. The dissociation probability is determined by the interplay of the rate of carrier dissociation jumps and the rate of the excess energy relaxation and is virtually independent of the sample temperature. The excess photon energy above the $S_1 \leftarrow S_0$/0–0 transition is considered to be transferred into intrasegmental vibronic energy and establishes, while dissipating, an important additional source of energy required for carriers to cross the potential barrier and to separate within the segment. The external electric field lowers the potential barrier for carrier separation and thus assists the dissociation of optical excitations. An important theory parameter is also the exciton binding energy, in polymers having an order of ~0.4 eV. The diffusive motion in the Coulomb potential in this theory is irrelevant since all processes occur inside the same conjugated chain segment.

Photoinduced excitons and bound polaron pairs themselves cannot create electric current. The free carriers involved in photocurrent (in conjugated polymers these are mostly charged polarons and bipolarons) are derived primarily from exciton dissociation [68]. The one-dimensional intrachain mobilities μ_0 of electrons and holes on isolated polymer chains free from interchain interactions are considerably higher than those in bulk materials. For instance, for holes in PPV, $\mu_0 \sim 0.5$ cm^2/V/s [90] dropping in the bulk materials to 10^{-4}–10^{-6} cm^2/V/s, mostly due to the barriers presented by domain and grain boundaries and, in the case of the electrons, also to deep trapping sites [91]. In almost all conjugated polymers (for exceptions see [82, 92]) the mobility of holes is much higher than that of electrons.

Photocurrent measurements are usually performed at sandwich structures containing thin (from some tens of nanometers to some micrometers) polymer films with asymmetric contacts providing effecting injection of electrons from a cathode and holes from an anode (see

Section 2.3). The current–voltage characteristic of such structures is usually asymmetric and depends on the illumination intensity much more strongly than in typical semiconductor photovoltaic structures (see Figure 5). Asymmetry of the current–voltage characteristic is caused by different work functions, and hence different contact barriers, for the cathode and anode, as well as by significantly different electron and hole mobilities [93]. Due to such asymmetry, an illuminated sandwich structure produces a photocurrent even in the absence of an applied bias [73, 92].

For many organic semiconductors, two types of relationships between the photocurrent and absorption spectra exist. If they correlate well, so that the maximum photocurrent is obtained for the most strongly absorbed light, the photocurrent response is said to be symbatic with the absorption spectrum. Under the opposite condition, when the photocurrent maxima occur for photon energies where the absorption is weakest, the photocurrent response is said to be antibatic. The type of photocurrent spectra depends on the applied bias voltage, the electrode through which it is illuminated, and the thickness of the polymer film (Fig. 6).

Free carrier photogeneration in conjugated polymers depends on the details of light absorption, exciton dissociation, and current injection from the contacts. Experiments on transient photoconductivity demonstrate the presence of two components of photocurrent, called intrinsic and extrinsic [68, 79]. They differ by the mechanism of free carrier generation, characteristic time, light intensity, electric field, and temperature dependences. Intrinsic photocarriers result from dissociation of photogenerated excitons by mechanisms characteristic for polymer chains themselves. They may include the influence of ambient temperature and applied electric field but not the interaction with interfaces, chemical defects, and other impurities not forming the polymer chain structure. The latter are responsible for the extrinsic photocurrent.

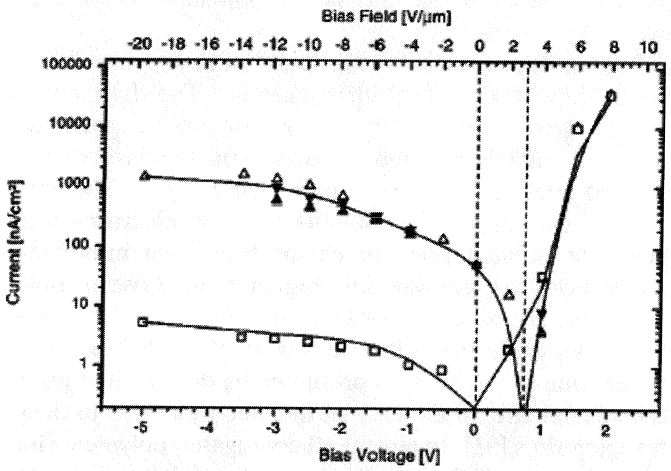

Figure 5. Current–voltage characteristics of a 255-nm-thick Au/arylamino-PPV/Al device. Squares represent currents without illumination conditions; triangles are data recorded under different illumination conditions. Illumination through Al was at $\lambda = 450$ nm (Δ). For illumination through Au $\lambda = 375$ nm (▲) and $\lambda = 485$ nm (▼) were used. Reprinted with permission from [73], K. Däubler et al., *Phys. Rev. B.*, 59, 1964 (1999). © 1999, American Physical Society.

Transient photoconductivity reveals fast (~100 ps or even less) and slower (~600 ps) components [75]. The magnitude of the fast component, usually related to the extrinsic photocurrent, is independent of temperature and linearly dependent on light intensity. It is linear in electric fields up to fields of a few times 10^4 V/cm. The slower component is proportional to the square root of the light intensity and has an activation temperature dependence with the activation energy ~100 mV. It is connected with the intrinsic photocurrent and, from its intensity dependence, is attributed to bipolarons [74], with account of their lower mobility compared with polarons.

Kinetics of photocurrent in PPV films studied in air and vacuum [79] also showed the presence of fast and slow components but in the time scale of seconds. In air the characteristic time of the slow component can be as long as several hours. This slow component, attributed to intrinsic processes, depends on the square root of the light intensity. It results from the interaction of the photogenerated polaron pairs with defects to create positive polarons. The restricted recombination of charge carriers, which is responsible for the slow buildup and decay kinetics, is interpreted as being due to the dispersive diffusion of positive polarons in a random density of negatively charged defects. The fast, extrinsic component is related to the thermal dissociation of excitons and subsequent creation of conducting positive polarons and immobile negative polarons. The decay of polaron pairs may be at the origin of such excitons, with one charge jumping to the adjacent chain to create an on-chain exciton. As exciton dissociation competes with geminate recombination this photocurrent rapidly reaches steady state and depends linearly upon optical power. In view of increased geminate pair dissociation in disordered media [94], resulting in temperature independence of the fast component proportional to light intensity, it has been suggested [79] that the linear picosecond response of [75] is also the intrinsic photocurrent. The higher the degree of energetic disorder, the faster the dissociation and the higher the quantum yield of mobile carriers.

Extrinsic processes play an important role in the explanation of the symbatic and antibatic spectra and some other characteristics of photocurrent. A comparative analysis of different photocurrent models is given in [76]. The models can be divided into two groups. The first group assumes that carrier generation is only successful within a narrow photoactive region, called the barrier region, close to one of the electrodes. It is not a true Schottky barrier but rather a thin barrier region of fixed width 10 nm, consisting of metal-oxide layers and

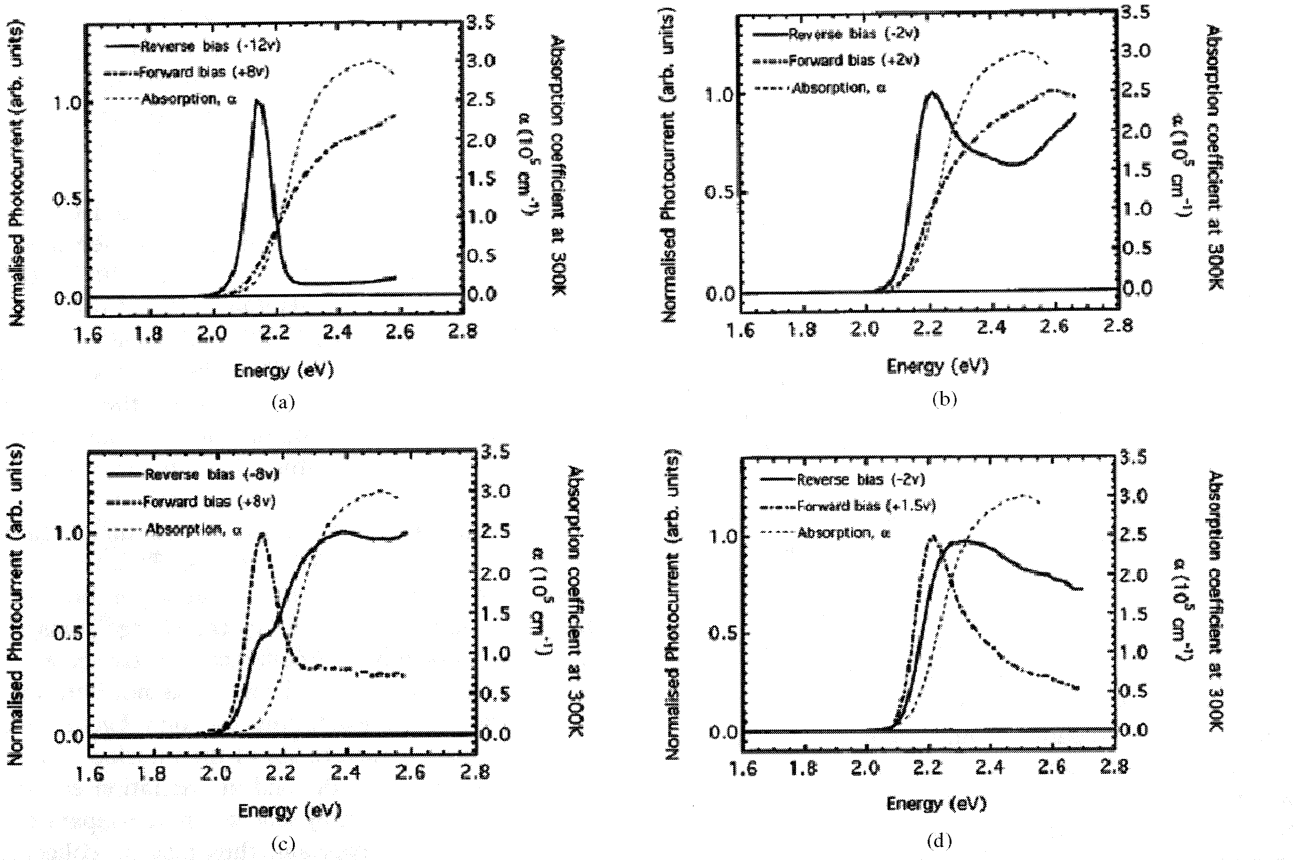

Figure 6. Photocurrent action spectra at room temperature for the ITO/MEH-PPV/Al diodes under forward bias (- · -) and reverse bias (———), with the room temperature absorption spectrum (- - - - -). Reprinted with permission from [76], M. G. Harrison et al., *Phys. Rev. B.*, **55**, 7831 (1997). © 1997, American Physical Society. (a) Thick (780 nm) polymer film, illumination through the ITO electrode; (b) thin (120 nm) polymer film, illumination through the ITO electrode; (c) thick film, illumination through the Al electrode; (d) thin film, illumination through the Al electrode.

an insulating, defective region of the polymer. In either case there is evidence of a thin, highly resistive layer resulting in a high local electric field at the barrier, which could assist exciton dissociation. In the model [95] most often used for the analysis of experimental data, light absorption in a polymer film followed by exciton diffusion toward the dissociation area near the barrier is taken into account. The second group of models contains an explicit solution of the diffusion equation, either for excitons or free charges, subject to various boundary conditions (see, e.g., [96]). These models give similar results explaining symbatic and antibatic photocurrent spectra but with a serious disagreement with experiment at low photon energies. A qualitative explanation of the symbatic and antibatic responses requires account of the internal filter effect from self-absorption inside the film.

From experimental results in sandwich structures it may be concluded that carrier photogeneration is an extrinsic process, following dissociation of excitons, either in the presence of oxygen molecules acting as electron traps, or at metal electrodes, into which an exciton may expel an electron [76] (in the case of a polymer with the *p*-type conductivity). When one carrier leaves an exciton pair for a contact electrode while the second one remains in a polymer film, the situation is called photoinjection for the remaining carriers. In an Al/poly(3-dodecylthiophene)/ITO structure illuminated from the Al contact at low bias voltages not exceeding ±5 V, photoinjection of holes was manifested as a considerable current growth in a direct branch compared with the dark current [93]. Experiments show [70] that the current component caused by carrier generation in the bulk is small compared with that caused by generation in the contact region. For reverse bias, this region in *p*-type polymers is located near the cathode electrode having the lower work function (for *n*-type polymers the situation is opposite [92]) since in this case the carriers with lower mobility can be directly removed into a contact.

Carrier dissociation in a sandwich structure with different contact work functions allows fabrication of large area polymer solar elements [97, 98]. Their drawback is a low conversion efficiency of order 10^{-3}–10^{-2}% for pure conjugated polymers [99] since carriers are collected only from the narrow layer directly adjacent to the contact where excitons dissociate. The low mobility of carriers (especially electrons in *p*-type polymers) prevents collection of photoexcited carriers. The small size of the dissociation area is one more reason for

the low conversion efficiency. All these negative factors stimulate a search for new ways of increasing the effectiveness of energy transformation, including embedding semiconducting, dielectric, or metallic nanoparticles into the matrix of a conjugated polymer.

5. EXPERIMENTAL INVESTIGATIONS OF POLYMER–NANOCRYSTAL COMPOSITES

5.1. Nonequilibrium Carriers in Nanocomposites

Embedding of semiconductor (e.g., CdS, CdSe) or dielectric (e.g., TiO_2) nanocrystals into a conjugated polymer matrix creates internal polymer/inorganic material interfaces stimulating extrinsic dissociation of light-emitted excitons and bound polaron pairs. Exciton dissociation is enhanced since it is energetically favorable for electrons to move from the polymer LUMO levels to the conduction band of the nanocrystals (Fig. 7). An important parameter in exciton dissociation is their diffusion length, which in polymers has the order of 5–15 nm [16]. For a high density of nanocrystals (exceeding 15–20% volume), percolation paths through the network of nanocrystals appear and additional electron transport absent in *n*-type polymers becomes possible. Electron mobility in the nanocrystal materials μ_s is essentially higher than in polymers. For instance, in TiO_2 $\mu_s \sim (0.1\text{–}1)$ $cm^2/V\,s$ [16], which is several orders of magnitude higher than in typical polymers. In most semiconductors in turn, μ_s is essentially higher than in TiO_2. Nanocrystals also provide the possibility of optical generation of carriers followed by the hole transitions into polymer. This process, considered in more detail in Section 7, is also energetically favorable since CdS, CdSe, and TiO_2 form the type-II band diagram (see Section 3) with most conducting

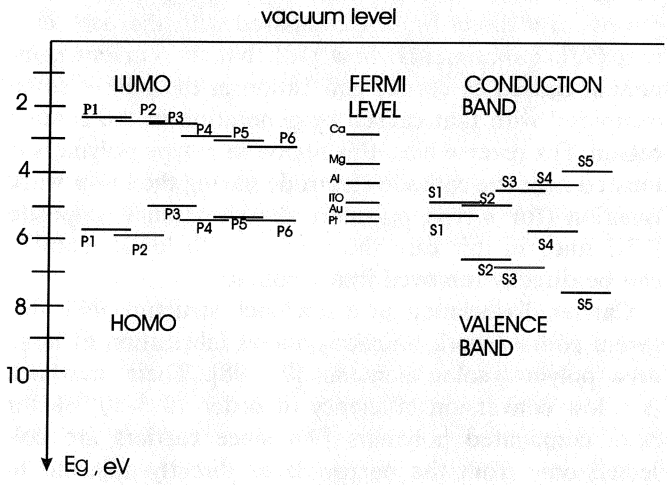

Figure 7. Relative energy band positions in major polymers and nanocrystals. P1—PVK, P2—*t*-Bu-PBD, P3—PPV, P4—arylamino-PPV, P5—MEH-PPV, P6—P3HT; S1—InAs, S2—CdSe, S3—CdS, S4—CdTe, S5—ZnS.

polymers. Therefore, nanocomposites can provide very effective separation of charges which in a pure polymers would be bound into excitons or bound polarons.

Photoconductivity and/or photovoltaic effects were experimentally investigated in a number of polymer–nanocrystal composites[2]: PPV/TiO_2 [39, 43, 101], MEH-PPV/TiO_2 [67, 102], LPPP/dye-sensitized TiO_2 [36, 103], PVK/dye-sensitized TiO_2 [36], PPV/dye-sensitized TiO_2 [36], MEH-PPV/CdSe [16, 19, 20, 104, 105], MEH-CN-PPV/CdSe [19, 106], DHeO-CN-PPV/CdSe [19, 106], P3HT/CdSe [107], MEH-PPV/CdS [58], 6FPBO/CdS [58], and PVK/CdS [108, 109]. The effectiveness of photoelectric devices is determined by the photocurrent quantum yield Q, the number of electrons in an external circuit per light quantum. This characteristic depends on the photon energy $E = \hbar\omega$ and in the short circuit scheme can be written as a product of three factors: $Q(E) = A(E)\kappa\varphi(E)$ where $A(E)$ is the fraction of photons absorbed, κ is the charge separation yield per absorbed photon, and $\varphi(E)$ is the charge transport efficiency, or probability of collecting the charge at contact. The charge separation efficiency κ is not determined by the energy of the excitation, but only by the energetic and electrical characteristics of the interface. The collection efficiency φ may depend on excitation energy, since different excitations may lead to charge-separated states with different lifetimes and thus may be collected with different efficiencies.

The photoluminescence efficiency Φ (number of photons emitted in photoluminescence per absorbed photon) of conjugated polymers depends on the fraction of absorbed photons that produce singlet excitons (the branching ratio η) as opposed to other species such as spatially separate polaron pairs, and the probability ε that singlet excitons will decay to the ground state by radiative emission: $\Phi = \eta\varepsilon$. This characteristic for pure polymers is in PPV $\Phi = 0.27$, in MEH-PPV $\Phi = 0.1$–0.15, in CN-PPV $\Phi = 0.35$–0.36, and in MEH-CN-PPV $\Phi = 0.48$ [110]. Measurements showed that, for example, for PPV $\varepsilon = 0.28$ [110], which means that η is close to unity, implying that the species produced by photoexcitation is predominantly the singlet exciton. Only after excitation of singlet excitons do approximately $\frac{3}{4}$ of them transform into a triplet state with subsequent nonradiative recombination. This fraction may vary from $\frac{3}{4}$ due to the change of efficiency of this transformation in different polymers. A considerable drop in this parameter in MEH-PPV is believed to be caused by a higher degree of ordering and, as a consequence, spreading of exciton charges over adjacent chains with ensuing nonradiative recombination. (The most likely interpretation is that another branching channel is added to the system, i.e., an exciton loss via charge separation which subsequently

[2] Standard chemical abbreviations of polymers used below are explained in the Appendix.

decays nonradiatively.) For PPV the parameter is seen to approach $\frac{3}{4}$. Given that the photoluminescence efficiency decrease is due to charge separation at the polymer–nanocrystal interface, the fraction of charge separation events per absorbed photon can be written $\Gamma = \eta\kappa$ where κ is the efficiency of charge separation of the state. Thus $\Gamma + \Phi = 1$, with all absorbed photons leading to either luminescence or charge separation. In general each term (Γ and Φ) is also dependent on the photon energy. Γ is determined by κ via geometric considerations (distribution of nanocrystals per unit volume, i.e., polymer–nanocrystal distance) and by the probability of exciton dissociation upon reaching an interface. In the case of nearly complete photoluminescence quenching, with all absorbed photons leading to singlet excitons which are capable of charge separation, $\kappa \simeq 1$, and thus all absorbed photons lead to charge separation. In conjugated polymers, in general, the efficiency of dissociation, κ, may be lower than unity, or there may be other nonradiative channels of decay available to an exciton upon reaching the interface, resulting in a less than complete photoluminescence quenching. This should really be the case if part of singlet excitons have enough time to transform into a triplet state where most of them recombine nonradiatively. However, if singlet excitons have time to dissociate at the nanocrystal interface before transforming into triplet or the interface causes decay of both singlet and triplet excitons, κ may be expected to be close to unity. Direct observations of complete photoluminescence quenching by microwave conductivity measurements [43] confirm that all excitons are converted into separated charges in composite PPV/TiO_2 with 20% TiO_2 and higher. Photoluminescence quenching provides evidence for charge transfer, because once the singlet exciton has been dissociated, it can no longer decay radiatively to the ground state (Fig. 8).

The effectiveness of charge separation at the polymer–nanocrystal interface plays a key role in the effectiveness

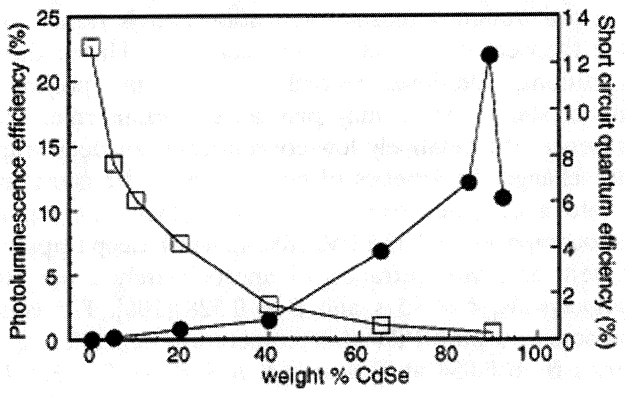

Figure 8. Photoluminescence efficiency (squares) and short-circuit quantum efficiency (circles) in the MEH-PPV/CdSe nanocomposite as a function of nanocrystal concentration. Reprinted with permission form [104], N. C. Greenham et al., *Synth. Met.*, 84, 545 (1997). © 1997, Elsevier Science.

of solar elements and photoconductors. Charge transfer from polymer to nanocrystal will be energetically favorable if $\chi^s - \chi^p > U - V$, where $\chi^{p,s}$ are the electron affinities (see Section 3), U is the Coulomb binding energy of a singlet exciton in the polymer, and V is the Coulomb energy associated with attraction between electron and hole in the final, charge-separated state. In general, U is significantly larger than V due to the increased average electron–hole separation in the charge-separated state. The difference in electron affinities between CdS, CdSe, and TiO_2 on the one hand and typical conducting polymers on the other (Fig. 9) is so high that the above-mentioned condition is always fulfilled, given that the typical exciton binding energy is only ~0.4 eV. Even the decrease in effective χ^s due to size quantization in nanocrystals will not significantly alter the charge transfer effectiveness. No such size dependence is observed in a MEH-PPV/CdSe nanocomposite with nanocrystals of 5 nm and less. There is also no evidence for an electron–polaron interaction that is affected by nanocrystal size [19].

One may distinguish three mechanisms of forming the mobile carriers in a polymer and nanocrystals. The first consists of exciton dissociation at the polymer–nanocrystal interface with direct transition of electrons to the conduction band of nanocrystal; the second includes energy transfer from the excited state of polymer to nanocrystals via the Förster mechanism (see, e.g., [69]) or with the reemission when a photon emitted in a polymer is absorbed in a nanocrystal, creating an excitation followed by hole transfer into the polymer. The third mechanism is related to direct light absorption in a nanocrystal and the hole transition to a polymer. The Förster mechanism is effective when excitation energies in the polymer and nanocrystal are close. The final effect of all three mechanisms is the creation of a free electron in a nanocrystal and of a positively charged mobile polaron in a polymer.

The effectiveness of charge transfer from polymer to nanocrystal depends to a great extent on conditions at the polymer–nanocrystal interface. Charge transfer is different for clean nanocrystals and those coated with a layer of TOPO molecules. A TOPO shell prevents direct charge transfer by forming a barrier of 11 Å thickness between the nanocrystal core and the polymer. At the same time, this barrier does not noticeably inhibit the Förster mechanism [16] if the conditions for energy transfer are fulfilled. Experiments on luminescence quenching in MEH-PPV/CdS and MEH-PPV/CdSe nanocomposites with bare and TOPO-coated nanocrystals [16] demonstrate considerable quenching as the nanocrystal density increases for bare nanocrystals of both CdS and CdSe. The behavior of TOPO-coated nanocrystals was quite different: quenching was observed for CdSe and was almost absent for CdS nanocrystals. Due to a much

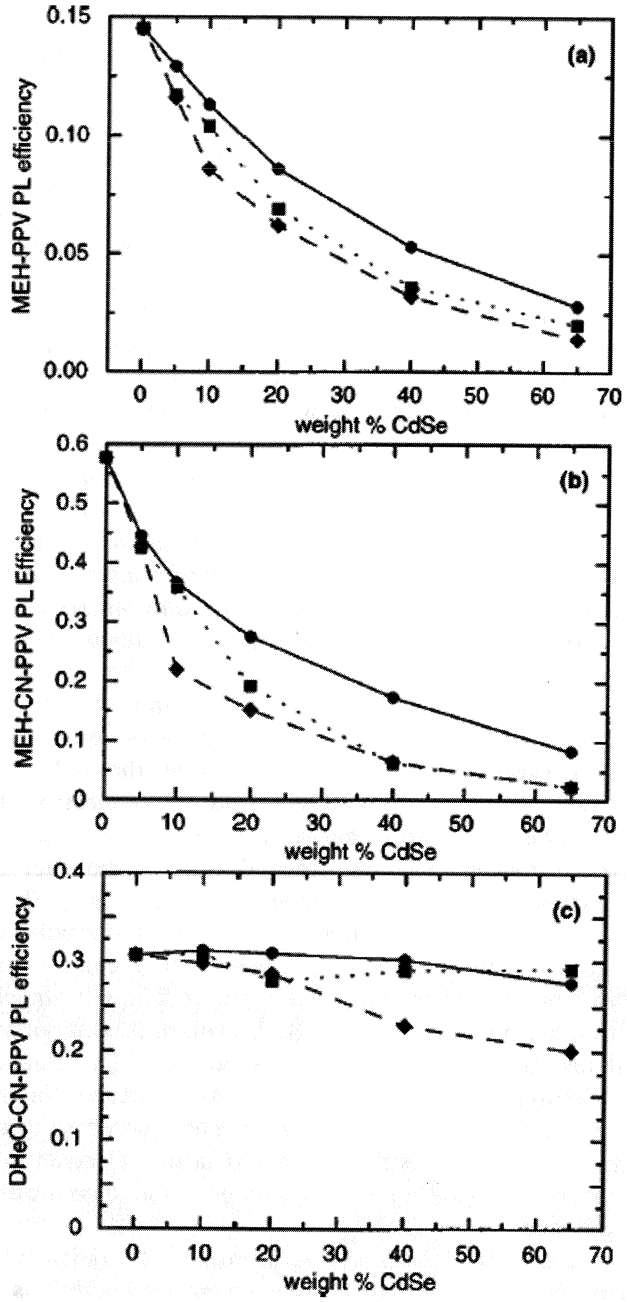

Figure 9. Photoluminescence efficiencies of blends of (a) MEH-PPV, (b) MEH-CN-PPV, and (c) DHeO-CN-PPV with CdSe nanocrystals of 2.5 (squares), 3.3 (circles), and 4.0 (diamonds) nm in diameter. Reprinted with permission from [19], D. S. Ginger and N. C. Greenham, *Phys. Rev. B.*, 59, 10622 (1999). © 1999, American Physical Society.

higher absorption coefficient of MEH-PPV at the wavelength 476.1 nm compared with nanocrystals, most of the light is absorbed by the polymer. With CdSe nanocrystals, there is a good overlap between the polymer emission spectrum and the nanocrystal absorption spectrum, and Förster exciton transfer occurs from polymer to nanocrystal. In contrast to the process of charge transfer, Förster transfer does not require wave-function overlap (tunneling) between the two materials and can therefore occur in the presence of a TOPO barrier which suppresses electron transfer to CdS.

A barrier at the polymer–nanocrystal interface may be created not only by the TOPO shell but also by the structure of the polymer itself. Comparison of the luminescence quenching in nanocomposites MEH-PPV/CdSe and MEH-CN-PPV/CdSe on the one hand and DHeO-CN-PPV/CdSe [19, 106] and CN-PPV/CdSe [20] on the other demonstrated a systematic influence of polymer structure on the character of polymer–nanocrystal interaction [19, 20, 104, 106] (see Fig. 9). The polymer DHeO-CN-PPV differs from MEH-PPV and MEH-CN-PPV by the presence of the dihexyloxy chains on both sides of the polymer backbone. It prevents a nanocrystal from approaching sufficiently closely the conjugated backbone to allow charge transfer. Although charge transfer is thermodynamically favorable, it is prevented from happening by a kinetic barrier. Similarly to the case of TOPO-coated nanocrystals, there remains the possibility of energy transfer via the Förster mechanism with subsequent nonradiative decay in the nanocrystal or hole transfer to the polymer. This results in luminescence quenching in DHeO-CN-PPV with the increase of CdSe nanocrystal concentration (Fig. 9c), which is much less than in MEH-PPV and MEH-CN-PPV. More effective charge transfer in MEH-PPV compared with DHeO-CN-PPV is confirmed also by the observation of positively charged polarons in the photoinduced absorption spectra in MEH-PPV/CdSe and their absence in DHeO-CN-PPV/CdSe [19].

5.2. Photoconductivity

Photoconductivity in a nanocomposite depends on the lifetime of nonequilibrium carriers determined by the recombination processes. Since separated electrons and holes for type-II structures are localized in different materials and separated by rather high potential barriers (at least several tenths of an eV) the recombination rate requires thermal activation and is rather low (see theoretical calculations in Section 7). Under these conditions, additional recombination at the polymer–nanocrystal interface may play an important role. The presence of a relatively low concentration of deep traps may change the kinetics of current decay, transforming it into a stretched exponential $I = I_0 \exp[-(t/\tau)^{\beta}]$. In nanocomposites MEH-PPV/CdSe in which deep traps are present at a concentration of approximately 1 per 100 nanocrystals, $\tau = 95$ s and $\beta = 0.328$ [106]. For comparison, in a pure PPV β is temperature dependent and varies from 0.054 at T near 0 K to 0.32 at $T = 325$ K; τ also depends on temperature varying from 0.5 s at 190 K up to the maximal value 220 s at 255 K [79].

In PPV/TiO_2 nanocomposites, the conductivity in TiO_2 nanocrystals relaxes in such a manner that half of the excited carriers recombine in 10 μs and 80% in 90 μs

[39, 43, 101]. The process of recombination between the spatially separated electrons and holes in the PPV/TiO_2 composite occurs in hundreds of nanoseconds to several microseconds. Recombination of the separated charges occurs in a complex manner with half of the initial signal amplitude decaying in 600 ns in a nonexponential fashion. The part of the decay after 800 ns can be well fitted to a sum of two exponentials with time constants of 4.3 and 80 μs and relative amplitudes of 0.7 and 0.3. The measured recombination time scales are significantly longer than the typical times for radiative or nonradiative decays of singlet excitons in the conjugated polymers [109]. The fact that free-charge-carrier decay in TiO_2 nanocrystals alone occurs much more slowly than the interfacial recombination process in composites suggests a longer time delay before hole transfer to the polymer.

To obtain high quantum yield of photocurrent, we need not only efficient charge separation but also efficient transport of the carriers to the electrodes without recombination. Recombination is minimized when the carriers are separated onto different materials, and both carriers have pathways to the appropriate electrode within the component of the film onto which they have been separated. At low concentrations of nanocrystals the size of the nanocrystal domains is small, so that only the few electrons generated on the larger nanocrystal domains very close to the cathode electrode (Al, Ca or Mg electrodes) will have a pathway to the electrode in *p*-type polymers. At higher concentrations, nanocrystals begin to form a connected network [16]. In this case, it becomes much more likely for an electron generated on a nanocrystal at an arbitrary position within the device to be able to find its way through the thickness of the device. The efficiency of collecting charge at a contact will depend on the site of charge separation in the film, since different locations are at different distances from the contact. The polymer phase is continuous throughout the composite, but only some fraction of the nanocrystals is in physical contact with other nanocrystals. Therefore, a path exists from any charge separation site in the composite for hole transport to the anode contact (ITO, Au), but there may not be such a path for the electrons in the nanocrystal (TiO_2, CdS, CdSe) to the cathode electrode. Furthermore, even if conducting pathways do exist for the electrons in the nanocrystals, they may not be transported efficiently through the network due to energetic barriers or grain boundaries between nanocrystals. Thus for *p*-type polymers, the magnitude of the short-circuit currents will be limited by electron transport through the nanocrystalline phase rather than by hole transport through the polymer phase. Charge transfer and recombination at the contacts of the device are not limiting factors in the quantum yields [43].

Comparison of the experimentally observed relaxation time in PPV/TiO_2 nanocomposites with the model of hopping conductivity in close-packed, ordered square lattice of nanocrystals indicates that only charge generated within one or two nanocrystal layers from the contact will have an appreciable probability of being collected [43].

The current–voltage characteristic (CVC) of nanocomposite structures has an asymmetric, rectifying character (as any CVC for contacts with different work functions) and depends on the light intensity. Figure 10 shows such a CVC for a MEH-PPV/CdSe nanocomposite (90 wt% CdSe) in the dark and under illumination. At 40 wt% of nanocrystals the photoluminescence is quenched by a factor of approximately 10. It is therefore likely that, in the presence of an internal field within the device, significantly more than 90% of the excitons are dissociated at an interface. Although the short-circuit quantum efficiency of this device is much larger than that of a pure MEH-PPV device, it is stil' more than a factor of 10 smaller than the maximum efficiency found in the device with 90 wt% CdSe. The improvement in efficiency between 40 and 90 wt% is largely due to improvement in electron transport, and the improvement in efficiency at lower concentrations is due to improvements in both charge separation and transport. The peak in efficiency at 90 wt% CdSe corresponds to a volume fraction of

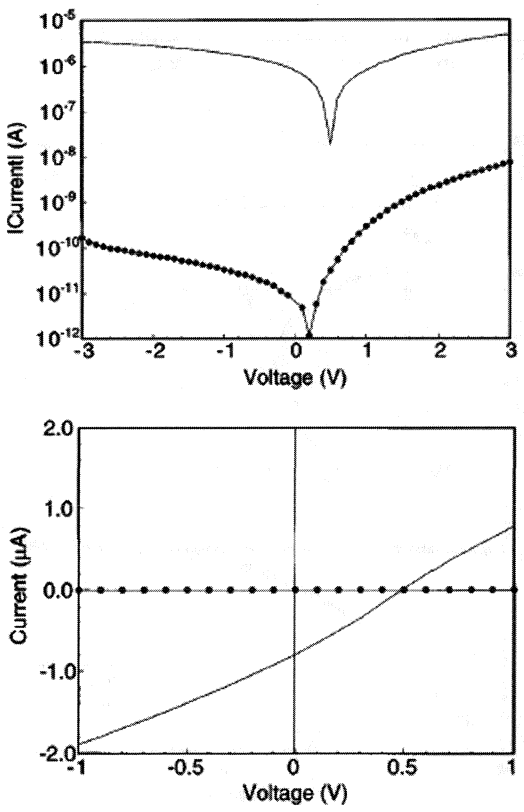

Figure 10. (a) Current–voltage curve for a device containing 90 wt% CdSe in the dark (circles) and under illumination at 514 nm (solid line). Reprinted with permission from [16], N. C. Greenham et al., *Phys. Rev. B.*, 54, 17628 (1996). © 1996, American Physical Society. (b) The same data for a smaller range of voltage, with the current on a linear axis.

nanocrystal of approximately 65%, at which point a good percolation path through both nanocrystal and polymer components is established.

Figure 11 shows the CVC for a polymer–dielectric composite MEH-PPV/TiO_2 with and without illumination [102], demonstrating the large photoresponse of the system. The I_{ph}/I_{dark} ratio under reverse bias is as high as 10^4 at -4.5 V with responsivity of ~50 mA/W at -9 V and $I_{dark} = 10$ nA. The intensity dependence of I_{ph} for input power 0.1 μW/cm^2–1 mW/cm^2 is linear over the entire voltage range. Figure 12 is an example of the CVC for another polymer matrix PPV/TiO_2 [39] having qualitatively similar properties.

The structures considered can be connected into an external circuit in different regimes. Figure 13 shows the band diagram of a structure under (a) short-circuit conditions, (b) open-circuit conditions (flat bands), and (c) forward bias electron injection. In the first case there is a built-in electric field in the film determined by the difference of contact work functions and film thickness. This field stimulates charge separation in nanocomposites. For a high concentration of nanocrystals, percolation phenomena exist, the hole current flows through the polymer matrix and the electron current—through the closely packed nanocrystals. The flat band conditions occur in the open circuit at very high illumination intensity when the open circuit voltage equal to the contact work-function difference is generated in the structure.

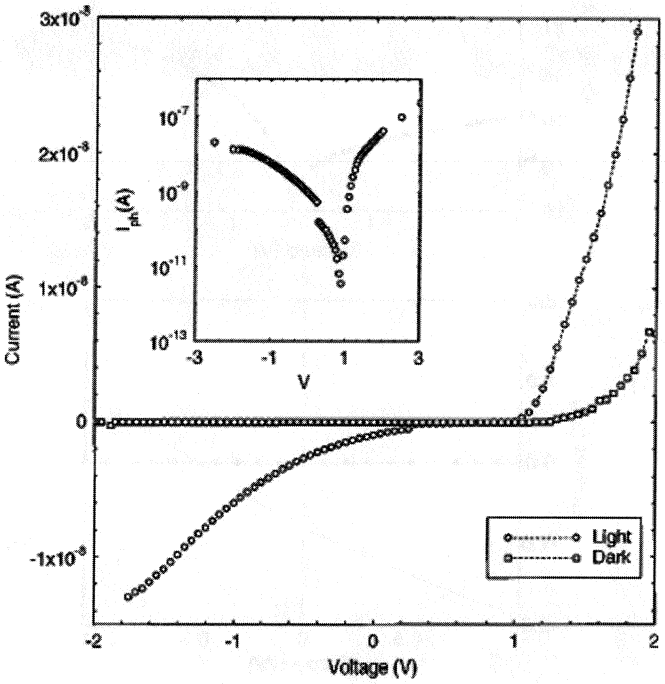

Figure 11. Current–voltage characteristics in the dark and white light (20 μW) of a device containing TiO_2/MEH-PPV composite. Reprinted with permission from [102], K. S. Narayan and Th. B. Singh, *Appl. Phys. Lett.*, 74, 3456 (1999). © 1999, American Institute of Physics. Inset is the current under illumination in the logarithmic scale vs voltage.

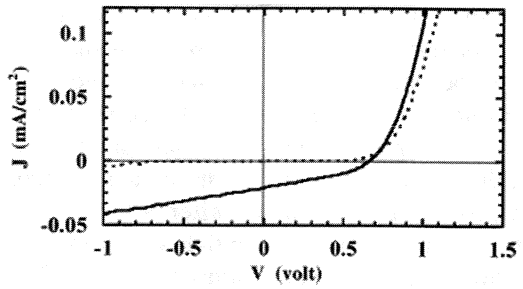

Figure 12. Current–voltage characteristics in the dark (dashed curve) and under white light illumination of 100 mW/cm^2 (solid curve) of a device containing TiO_2/PPV composite. Reprinted with permission from [39], J. S. Salafsky et al., *Chem. Phys. Lett.*, 290, 297 (1998). © 1998, Elsevier Science.

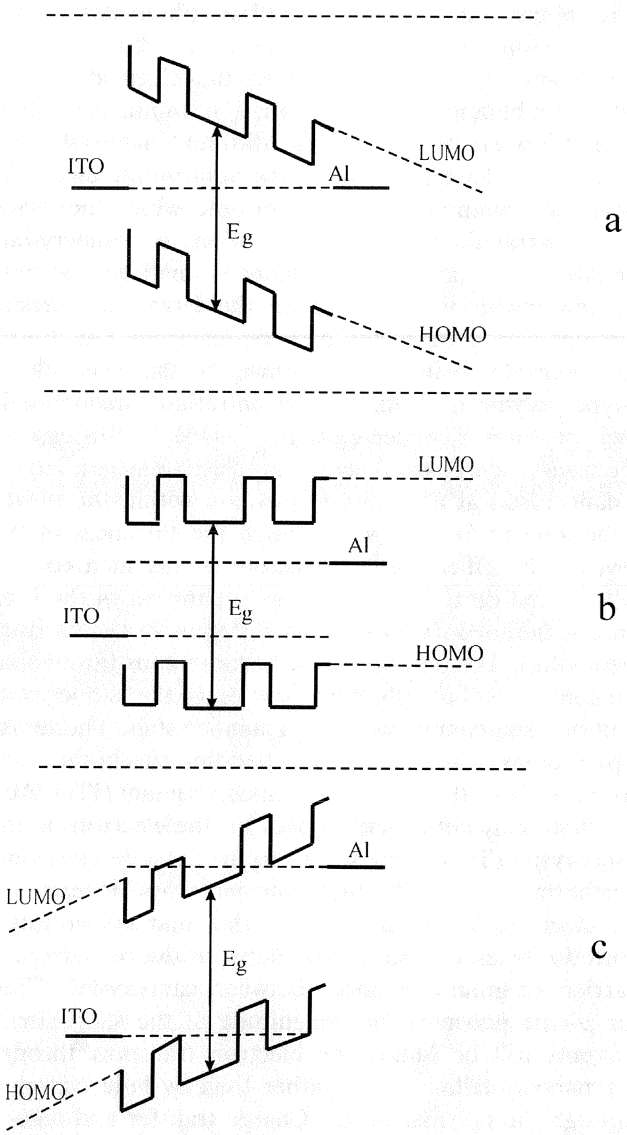

Figure 13. Schematic band diagrams in a section of single layer conjugated polymer devices embedded by nanocrystals at various values of forward bias (in respect to ITO). (a) Short-circuit conditions, (b) open-circuit (flat band) conditions, (c) forward bias with electron injection.

The experimentally determined open-circuit voltage for different structures with the same combination of contacts ITO–Al (with the work-function difference 0.55–0.65 eV) are in MEH-PPV/CdSe 0.5–0.6 V [16], in PPV/TiO_2 0.65 V [43], in MEH-PPV/ TiO_2 ~ 0.8 V [102].

If a sample is illuminated under applied bias, current flows due to both injection and optical generation of car-

[102]. Model calculations [95] at different values of the diffusion length for excitons (or free carriers) give a qualitative agreement with experiment but with the same discrepancy at large wavelengths as in pure polymer [76]. Antibatic spectral dependences were also observed in the PPV/TiO_2 structure [43].

Embedding CdSe and TiO_2 nanoparticles increases

Continued

Abbreviations	Name	Structural formula
P3DDT	poly(3-dodecylthiophene)	
PEO	poly(ethylene oxide)	CH_3-[CH_2-O-CH_2]n-CH_3
PAH	poly(allylamine)hydrochloride	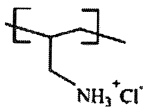
PLMA	poly(*n*-lauryl methacrylate)	$H_2C{=}C(CH_3)CO_2(CH_2)_{11}CH_3$
TPB	tetraphenylbenzidine	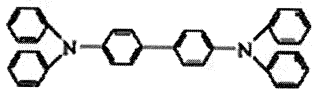
F6BT	poly[(9,9-dihexylfluorenyl-2,7-diyl)-co-(1,4-{benzo-[2,19,3]thiadiazole})]	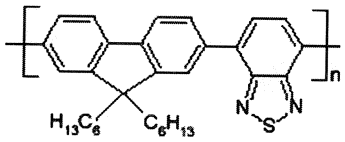
t-Bu-PBD	oxidiazole derivative: 2-(4-biphenylyl)-5-(4-tert-butylphenyl)-1,3,4-oxadiazole	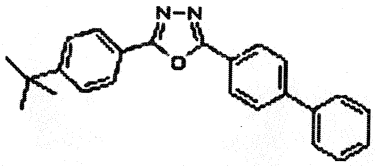
$RuL_2(NCS)_2$	*cis*-X_2bis(2,2′-bipyridyl-4,4′-dicarboxylate) ruthenium(II) (X = SCN^-) dye	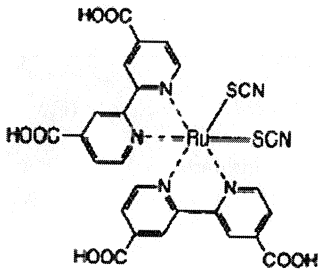
TOPO	tri-*n*-octylphosphine-oxide	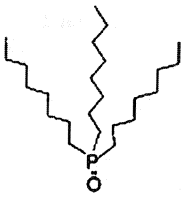

REFERENCES

1. "Organic Electroluminescent Materials and Devices" (S. Miyata and H. S. Nalwa, Eds.), Gordon & Breach, New York, 1997.
2. R. H. Friend, R. W. Gymer, A. B. Holmes, J. H. Burroughes, R. N. Marks, C. Taliani, D. D. C. Bradley, D. A. Dos Santos, J. L. Bredas, M. Logdlund, and W. R. Salaneck, *Nature* 397, 121 (1999).
3. T. R. Hebner, C. C. Wu, D. Marcy, M. H. Lu, and J. C. Sturm, *Appl. Phys. Lett.* 72, 519 (1999).
4. Y.-S. Shon, W. P. Wuelfing, and R. W. Murray, *Langmuir* 17, 1255 (2001).
5. S. V. Gaponenko, "Optical Properties of Semiconductor Nanocrystals." Cambridge Univ. Press, Cambridge, UK, 1998.
6. C. B. Murray, C. R. Kagan, and M.G. Bawendi, *Annu. Rev. Mater. Sci.* 30, 545 (2000).
7. V. K. La Mer and R. H. Dinegar, *J. Amer. Chem. Soc.* 72, 4847 (1950).
8. I. M. Lifshits and V. V. Slesov, *Sov. Phys. JETP* 35, 479 (1958).
9. X. Peng, J. Wickham, and A. P. Alivisatos, *J. Amer. Chem. Soc.* 120, 5343 (1998).
10. C. B. Murray, D. J. Norris, and M. G. Bawendi, *J. Amer. Chem. Soc.* 115, 8706 (1993).
11. M. A. Hines and P. Guyot-Sionnest, *J. Phys. Chem.* 100, 468 (1996).
12. M. L. Steigerwald, A. P. Alivisatos, J. M. Gibson, T. D. Harris, A. R. Kortan et al., *J. Amer. Chem. Soc.* 110, 3046 (1988).
13. J. G. Winiarz, L. Zhang, M. Lal, C. S. Friend, and P. N. Prasad, *Chem. Phys.* 245, 417 (1999).
14. N. Herron, Y. Wang, and J. Eckert, *J. Amer. Chem. Soc.* 112, 1322 (1990).
15. T. Masui, K. Fujiwara, K. Machida, G. Adachi, T. Sakata, and H. Mori, *Chem. Mater.* 9, 2197 (1997).
16. N. C. Greenham, X. Peng, and A. P. Alivisatos, *Phys. Rev. B* 54, 17628 (1996).
17. M. P. Pileni, in "Nanoscale Materials in Chemistry" (K. J. Klabunde, Ed.), p. 61. Wiley, New York, 2001.
18. B. O. Dabbousi, M. G. Bawendi, O. Onitsuka, and M. F. Rubner, *Appl. Phys. Lett.* 66, 1316 (1995).
19. D. S. Ginger and N. C. Greenham, *Phys. Rev. B* 59, 10622 (1999).
20. D. S. Ginger and N. C. Greenham, *Synth. Metals* 101, 425 (1999).
21. H. Mattossi, L. H. Radzilowski, B. O. Dabbousi, E. L. Thomas, M. G. Bawendi, and M. F. Rubner, *J. Appl. Phys.* 83, 7965 (1998).
22. H. Mattossi, L. H. Radzilowski, B. O. Dabbousi, D. E. Fogg, R. R. Schrock, E. L. Thomas, M. F. Rubner, and M. G. Bawendi, *J. Appl. Phys.* 86, 4390 (1999).
23. C. Wang, W. X. Zhang, X. F. Qian, X. M. Zhang, Y. Xie, and Y. T. Qian, *Mater. Chem. Phys.* 60, 99 (1999).
24. D. Ingert, N. Feltin, L. Levy, P. Gouzert, and M. P. Pileni, *Adv. Mater.* 11, 220 (1999).
25. F. V. Mikulec, M. Kuno, M. Bennati, D. A. Hall, R. G. Griffin, and M. G. Bawendi, *J. Amer. Chem. Soc.* 122, 2532 (2000).
26. C. B. Murray, S. Sun, W. Gaschler, H. Doyle, T. A. Betley, and C. R. Kagan, *IBM J. Res. Dev.* 45, 47 (2001).
27. O. I. Micic, J. R. Sprague, C. J. Curtis, K. M. Jones, and A. J. Nozik, *J. Phys. Chem.* 98, 4966 (1994).
28. A. A. Guzelian, J. E. Bowen Katari, A. V. Kadavanich et al., *J. Phys. Chem.* 100, 7212 (1996).
29. A. A. Guzelian, U. Banin. A. V. Kadavanich, X. Peng, and A. P. Alivisatos, *Appl. Phys. Lett.* 69, 1432 (1996).
30. J. F. Janik, R. L. Wells, J. L. Coffer, J. V. St-John, W. T. Pennington, and G. L. Schimek, *Chem. Mater.* 10, 1613 (1998).
31. S. Schulz and W. Assenmache, *Mater. Res. Bull.* 34, 2053 (1999).
32. J. R. Heath, J. J. Shiang, and A. P. Alivisatos, *J. Chem. Phys.* 101, 1607 (1994).
33. K. A. Littau, P. J. Szajowski, A. J. Miller, A. R. Kortan, and L. E. Brus, *J. Phys. Chem.* 97, 1224 (1993).
34. Y. Wang, A. Suna, W. Mahler, and R. Kasowski, *J. Chem. Phys.* 87, 7315 (1987).
35. R. Könenkamp, P. Hoyer, and A. Wahi, *J. Appl. Phys.* 79, 7029 (1996).
36. T. K. Däubler, I. Glowacki, U. Scherf, J. Ulanski, H.-H. Hörhold, and D. Neher, *J. Appl. Phys.* 86, 6915 (1999).
37. P. K. H. Ho, J.-S. Kim, N. Tessler, and R. H. Friend, *J. Chem. Phys.* 115, 2709 (2001).
38. F. Hide, B. J. Schwartz, M. A. Diaz-Garcia, and A. J. Heeger, *Chem. Phys. Lett.* 256, 424 (1996).
39. J. S. Salafsky, W. H. Lubberhuizen, and R. E. I. Schropp, *Chem. Phys. Lett.* 290, 297 (1998).
40. L. Bakueva, S. Musikhin, and E. H. Sargent, 1st IEEE Conf. on Nanotechnology, Maui 2001, Proceedings, p. 437.
41. M. Nazeeruddin et al., *Helv. Chim. Acta* 73, 1788 (1990).
42. E. Scolan and C. Sanchez, *Chem. Mater.* 10, 3217 (1998).
43. J. S. Salafsky, *Phys. Rev. B* 59, 10885 (1999).
44. S. Monticone, R. Tufeu, A. V. Kanaev, E. Scolan, and C. Sanchez, *Appl. Surf. Sci.* 162–163, 565 (2000).
45. "Handbook of Physical Quantities" (I. S. Grigoriev, and E. Z. Meilikhov, Eds.). CRC Press, Boca Raton, FL, 1997.
46. M. C. Schlamp, X. Peng, and A. P. Alivisatos, *J. Appl. Phys.* 82, 5837 (1997).
47. X. Peng, M. C. Schlamp, A. V. Kadavanich, and A. P. Alivisatos, *J. Amer. Chem. Soc.* 119, 7019 (1997).
48. B. O. Dabbousi, J. Rodriguez-Viejo, F. V. Mikulec, J. R. Heine, and H. Matoussi, *J. Phys. Chem. B* 101, 9463 (1997).
49. J. Lee, V. C. Sundar, J. R. Heine, M. G. Bawendi, and K. F. Jensen, *Adv. Mater.* 12, 1102 (2000).
50. M. Danek, K. F. Jensen, K. F. Murray, C. B. Murray, and M. G. Bawendi, *Chem. Mater.* 8, 173 (1996).
51. N. Tessler, V. Medvedev, M. Kazes, S.-H. Kan, and U. Banin, *Science* 295, 1506 (2002).
52. A. Mews, A. Eychmüller, M. Giersig, D. Schooss, and H. Weller, *J. Phys. Chem.* 98, 934 (1994).
53. S. V. Kershaw, M. Burt, M. Harrison, A. Rogach, H. Weller, and A. Eychmüller, *Appl. Phys. Lett.* 75, 2694 (1999).
54. Y. W. Cao and U. Banin, *J. Amer. Chem. Soc.* 122, 9692 (2000).
55. Y. Yang, S. Xue, S. Liu, J. Huang, and J. Shen, *Appl. Phys. Lett.* 69, 377 (1996).
56. P. W. M. Blom, H. F. M. Schoo, and M. Matters, *Appl. Phys. Lett.* 73, 3914 (1998).
57. H.-M. Xiong, X. Zhao, and J.-S. Chen, *J. Phys. Chem. B* 105, 10169 (2001).
58. K. S. Narayan, A. G. Manoj, J. Nanda, and D. D. Sarma, *Appl. Phys. Lett.* 74, 871 (1999).
59. D. Decher, *Science* 277, 1232 (1997).
60. M. Gao, C. Lesser, S. Kirstein, H. Möhwald, A. L. Rogach, and H. Weller, *J. Appl. Phys.* 87, 2297 (2000).
61. C. B. Murray, C. R. Kagan, and M. G. Bawendi, *Science* 270, 1335 (1995).
62. V. S. Fomenko, "Handbook of Thermionic Properties: Electronic Work Functions and Richardson Constants of Elements and Compounds." Plenum Press Data Division, New York, 1966.
63. Y.-E. Kim, H. Park, and J.-J. Kim, *Appl. Phys. Lett.* 69, 599 (1996).
64. I. D. Parker and H. H. Kim, *Appl. Phys. Lett.* 64, 1774 (1994).
65. B. Masenelli, E. Tutis, M. N. Bussac, and L. Zuppiroli, *Synth. Metals* 122, 141 (2001).
66. L. Bakueva, S. Musikhin, E. H. Sargent, and A. Shik, in "Abstracts of MRS Fall Meeting," Boston 2001, p. 541.
67. A. C. Arango, S. A. Carter, and P. J. Brock, *Appl. Phys. Lett.* 74, 1698 (1999).
68. "Organic Electron Materials. Conjugated Polymers and Low Molecular Weight Organic Solids" (R. Farchioni and G. Grosso, Eds.). Springer, Berlin, 2001.
69. M. Pope and C. E. Swenberg, "Electronic Processes in Organic Crystals and Polymers." Oxford Univ. Press, London, 1999.

70. S. Barth, H. Bässler, H. Rost, and H. H. Hörold, *Phys. Rev. B* 56, 3844 (1997).
71. G. L. J. A. Rikken, D. Braun, E. G. J. String, and R. Demandt, *Appl. Phys. Lett.* 65, 219 (1994).
72. S. Barth and H. Bässler, *Phys. Rev. Lett.* 79, 4445 (1997).
73. T. K. Däubler, D. Neher, H. Rost, and H. H. Hörhold, *Phys. Rev. B* 59, 1964 (1999).
74. C. H. Lee, G. Yu, and A. J. Heeger, *Phys. Rev. B* 47, 15543 (1993).
75. C. H. Lee, G. Yu, D. Moses, and A. J. Heeger, *Phys. Rev. B* 49, 2396 (1994).
76. M. G. Harrison, J. Grüner, and G. C. W. Spencer, *Phys. Rev. B* 55, 7831 (1997).
77. E. Frankevich, A. Zakhidov, K. Yoshino, Y. Maruyama, and K. Yakushi, *Phys. Rev. B* 53, 4498 (1996).
78. M. Yan, L. J. Rothberg, F. Papadimitrakopoulos, M. E. Galvin, and T. M. Miller, *Phys. Rev. Lett.* 72, 1104 (1994).
79. B. Delieu, J. Wéry, S. Lefrant, and J. Bullot, *Phys. Rev. B* 57, 9118 (1998).
80. N. Kirova and S. Brazovskii, *Synth. Metals* 85, 143 (1997).
81. C. Y. Lee, J. Y. Park, Y. W. Park, D. Moses, A. J. Heeger, T. Noguchi, and T. Ohnishi, *Synth. Metals* 101, 444 (1999).
82. F. Feller and A. P. Monkham, *Synth. Metals* 116, 149 (2001).
83. E. K. Miller, D. Yoshida, C. Y. Yang, and A. J. Heeger, *Phys. Rev. B* 59, 4661 (1999).
84. J. J. Halls, K. Pichler, R. H. Friend, and Moratti, *Synth. Metals* 77, 277 (1996).
85. L. Onsager, *Phys. Rev.* 54, 554 (1938).
86. H. Scher and S. Rackovsky, *J. Chem. Phys.* 81, 1994 (1984).
87. D. Moses, J. Wang, G. Yu, and A. J. Heeger, *Phys. Rev. Lett.* 80, 2685 (1998).
88. V. I. Arkhipov, E. V. Emelianova, and H. Bässler, *Phys. Rev. Lett.* 82, 1321 (1999).
89. V. I. Arkhipov, E. V. Emelianova, S. Barth, and H. Bässler, *Phys. Rev. B* 61, 8207 (2000).
90. R. J. O. Hoofman, M. P. de Haas, L. D. A. Siebbeles, and J. M. Warman, *Nature* 392, 54 (1998).
91. H. Antoniadis, M. A. Abkowitz, and B. R. Hsieh, *Appl. Phys. Lett.* 65, 2030 (1994).
92. F. Feller and A. P. Monkhan, *Appl. Phys. Lett.* 76, 664 (2000).
93. S. B. Lee, K. Yoshino, J. Y. Park, and Y. W. Park, *Phys. Rev. B* 61, 2151 (2000).
94. U. Albrecht and H. Bässler, *Chem. Phys. Lett.* 235, 389 (1995).
95. A. K. Ghosh, D. L. Morel, T. Feng, R. F. Shaw, and C. A. Rowe, *J. Appl. Phys.* 45, 230 (1974).
96. A. K. Ghosh and T. Feng, *J. Appl. Phys.* 49, 5982 (1978).
97. K. Yoshino, K. Tada, A. Fujii, E. M. Conwell, and A. A. Zakhidov, *IEEE Trans. Electron Devices* 44, 1315 (1997).
98. C. J. Brabec, N. S. Sariciftci, and J. C. Hummelen, *Adv. Funct. Mater.* 11, 15 (2001).
99. C. J. Brabec and S. N. Sariciftci, *Monatsh. Chem. Chem. Month.* 132, 421 (2001).
100. N. S. Sariciftci, *Curr. Opin. Solid State Mater. Sci.* 4, 373 (1999).
101. J. S. Salafsky, H. Kerp, and R. E. I. Schropp, *Synth. Metals* 102, 1256 (1999).
102. K. S. Narayan and Th. B. Singh, *Appl. Phys. Lett.* 74, 3456 (1999).
103. M. Kocher, T. K. Däubler, E. Harth, U. Scherf, A. Gügel, and D. Neher, *Appl. Phys. Lett.* 72, 650 (1998).
104. N. C. Greenham, X. Peng, and A. P. Alivisatos, *Synth. Metals* 84, 545 (1997).
105. M. M. Erwin, A. V. Kadavanich, J. McBride, T. Kippeny, S. Pennycook, and S. J. Rosenthal, *Eur. Phys. J. D* 16, 275 (2001).
106. D. S. Ginger and N. C. Greenham, *Synth. Metals* 124, 117 (2001).
107. W. U. Huynh, X. Peng, and A. P. Alivisatos, *Adv. Mater.* 11, (1999).
108. Y. Wang and N. Herron, *J. Lumin.* 70, 48 (1996).
109. J. G. Winiarz, L. Zhang, M. Lal, C. S. Friend, and P. N. Prasad, *Chem. Phys.* 245, 417 (1999).
110. N. C. Greenham, I. D. W. Samuel, G. R. Hayes, R. T. Phillips, Y. A. R. R. Kessener, S. C. Moratti, A. B. Holmes, and R. H. Friend, *Chem. Phys. Lett.* 241, 89 (1995).
111. G. Yu and A. J. Heeger, *J. Appl. Phys.* 78, 4510 (1995).
112. S. Monticone, R Tufeu, A. V. Kanaev, E. Scolan, and C. Sanchez, *Appl. Surf. Sci.* 162–163, 565 (2000).
113. W. U. Huynh, J. J. Dittmer, and A. P. Alivisatos, *Science* 295, 2425 (2002).
114. "Electroluminescence I. Semiconductors and Semimetals" (G. Mueller, Ed.), Vol. 64. Academic Press, San Diego, 2000.
115. "*Electroluminescence II. Semiconductors and Semimetals*" (G. Mueller, Ed.), Vol. 65. Academic Press, San Diego, 2000.
116. "Handbook of Conducting Polymers" (T. A. Skotheim and R. L. Elsenbaumer, Eds.). Dekker, New York, 1998.
117. H.-K. Shim and J.-I. Jin, *Adv. Polym. Sci.* 158, 193 (2002).
118. J. Zhang, X. Ju, B.-J. Wang, Q.-S. Li, T. Liu, and T.-D. Hu, *Synth. Met.* 118, 181 (2001).
119. S. A. Carter, J. C. Scott, and P. J. Brock, *Appl. Phys. Lett.* 71, 1145 (1997).
120. Y. K. Kim, K. Y. Lee, O. K. Kwon, D. M. Shin, B. C. Sohn, and J. H. Choi, *Synth. Met.* 111–112, 207 (2000).
121. P. K. H. Ho, J.-S. Kim, N. Tessler, and R. H. Friend, *J. Chem. Phys.* 115, 2709 (2001).
122. L. Bozano, S. E. Tuttle, S. A. Carter, and P. J. Brock, *Appl. Phys. Lett.* 73, 3911 (1998).
123. W.-P. Chang and W.-T. Whang, *Polymer* 37, 4229 (1996).
124. A. V. Vannikov, A. D. Grishina, M. G. Tedoradze, V. A. Kolesnikov, and M. A. Brusentseva, *J. Photochem. Photobiol. A* 142, 67 (2001).
125. L. Bakueva, S. Musikhin, and E. H. Sargent, *J. Nanosci. Nanotech.* 1, 457 (2001).
126. S. Musikhin, L. Bakueva, E. H. Sargent, and A. Shik, *J. Appl. Phys.* 91, 6679 (2002).
127. V. Bliznyuk, B. Ruhstaller, P. J. Brock, U. Scherf, and S. A. Carter, *Adv. Mater.* 11, 1257 (1999).
128. X. M. Ding, L. M. Hung, L. F. Cheng, Z. B. Deng, X. Y. Hou, C. S. Lee, and S. T. Lee, *Appl. Phys. Lett.* 76, 2704 (2000).
129. L. Bakueva, D. Matheson, S. Musikhin, and E. H. Sargent, *Synth. Met.* 126, 207 (2002).
130. E. E. Moore and D. Yaron, *J. Chem. Phys.* 109, 6147 (1998).
131. G. G. Milliaras, J. R. Salem, P. J. Brock, and J. C. Scott, *Phys. Rev. B* 58, R13411 (1998).
132. A. Yokozawa and Y. Miyamoto, *Appl. Phys. Lett.* 73, 1122 (1998).
133. M. Gao, B. Richter, S. Kirstein, and H. Möhwald, *J. Phys. Chem.* 102, 4096 (1998).
134. W. Chen, D. Grouquist, and J. Roark, *J. Nanosci. Nanotech.* 2, 47 (2002).
135. N. P. Gaponik, D. V. Talapin, and A. L. Rogach, *Phys. Chem. Chem Phys.* 1, 1787 (1999).
136. N. P. Gaponik, D. V. Talapin, A. L. Rogach, and A. Eychmüller, *J. Mater. Chem.* 10, 2163 (2000).
137. Y. Yang, J. Huang, S. Liu, and J. Shen, *J. Mater. Chem.* 7, 131 (1997).
138. J. Ji and J. L. Coffer, *J. Phys. Chem. B* 106, 3860 (2002).
139. D. S. Ginger and N. C. Greenham, *J. Appl. Phys.* 87, 1361 (2000).
140. B. I. Shklovski and A. L. Efros, "Electronic Properties of Doped Semiconductors." Springer, Berlin, 1979.
141. A. D. Pomogailo, A. S. Rozenberg, and U. E. Uflyand, "Nanoscale Metal Particles in Polymers." Khimiya, Moscow, 2000 [in Russian].
142. D. Y. Godovsky, *Adv. Polymer Sci.* 153, 163 (2000).
143. A. Shik, S. Yu, E. Johnson, H. Ruda, and E. H. Sargent, *Solid-State Electron.* 46, 61 (2002).
144. R. Ferreira and G. Bastard, *Appl. Phys. Lett.* 74, 2818 (1999).
145. Y. Toda, O. Moriwaki, M. Nishioka, and Y. Arakawa, *Phys. Rev. Lett.* 82, 4114 (1999).
146. S. Marcinkevicius and R. Lean, *Phys. Scripta T* 79, 79 (1999).

147. L. D. Landau and E. M. Lifshits, "Electrodynamics of Continuous Media." Pergamon Press, New York, 1984.
148. M. A. Lampert and P. Mark, "Current Injection in Solids." Academic Press, San Diego, 1970.
149. L. Bakueva, A. Shik, S. Yu, H. Ruda, and E. H. Sargent, in "197th Meeting of the Electrochemical Society," Toronto, 2000, Book of Abstracts, # 1027.
150. A. Shik, H. Ruda, and E. H. Sargent, *Nanotechnology* 12, 523 (2001).
151. A. Shik, H. Ruda, and E. H. Sargent, *J. Appl. Phys.* 88, 3448 (2000).
152. G. Sergeev, V. Zagorsky, M. Petrukhin, S. Zavialov, E. Grigor'ev, and L. Thakhtenberg, *Anal. Commun.* 34, 113 (1997).
153. G. Gerasimov, E. Grigor'ev, and A. Grigor'ev, *Khim. Fiz.* 17, 180 (1998) [in Russian].
154. "Single Charge Tunneling" (H. Grabet and M. H. Devoret, Eds.). Plenum Press, New York, 1992.
155. D. Klein, R. Roth, A. Lim, A. P. Alivisatos, and P. L. McEuen, *Nature* 389, 699 (1997).
156. M. Chen and W. Porod, *J. Appl. Phys.* 78, 1050 (1995).
157. A. Ekimov, *J. Lumin.* 70, 1 (1996).
158. C. B. Murray, C. R. Kagan, and M. G. Bawendi, *Science* 270, 1335 (1995).
159. W. Shenton, D. Pum, U. Sleytr, and S. Mann, *Nature* 389, 585 (1997).
160. C. A. Mirkin, R. L. Letsinger, R. C. Mucic, and J. J. Storhoff, *Nature* 382, 607 (1996).
161. A. P. Alivisatos, X. G. Peng, and T. E. Wilson, *Nature* 382, 609 (1996).
162. L. Bakueva, S. Musikhin, E. H. Sargent and S. Schulz, 2nd. IEEE Conf. on Nanotechnology, Washington 2002, Proceedings, p. 181.